Geographical dependence observed in blocking high influence on the stratospheric variability through enhancement and suppression of upward planetary-wave propagation

Kazuaki Nishii* (nishii@atmos.rcast.u-tokyo.ac.jp)

Hisashi Nakamura* (hisashi@atmos.rcast.u-tokyo.ac.jp)

Graduate School of Science, University of Tokyo, Tokyo, Japan

7-3-1 Hongo Bunkyo-ku Tokyo, 113-0033, Japan

Yvan J. Orsolini (orsolini@nilu.no)

Norwegian Institute for Air Research, Kjeller, Norway; also at Bjerknes Centre for Climate Research, Norway

NILU, PO Box 100, N-2027 Kjeller, Norway

*Current affiliation: Research Center for Advanced Science and Technology, University of Tokyo.

Corresponding author address: Kazuaki Nishii, Research Center for Advanced Science and Technology, University of Tokyo, 4-6-1 Komaba, Meguro-ku, Tokyo, 153-8904, Japan.

Submitted to JCLIM, December 2010, revised June 2011, accepted July 2011.

Abstract

Previous studies have suggested the importance of blocking high (BH) development for the occurrence of stratospheric sudden warming (SSW), while there is a recent study that failed to identify their statistical linkage. Through composite analysis applied to high-amplitude anticyclonic anomaly events observed around every grid point over the extratropical Northern Hemisphere, the present study reveals distinct geographical dependence of BH influence on upward propagation of planetary waves (PWs) into the stratosphere. Tropospheric BHs that develop over the Euro-Atlantic sector tend to enhance upward PW propagation, leading to the warming in the polar stratosphere and, in some occasions, to major SSW events. In contrast, the upward PW propagation tends to be suppressed by BHs developing over the western Pacific and the Far East, resulting in the polar stratospheric cooling. This dependence is found to arise mainly from the sensitivity of the interference between the climatological PWs and upward-propagating Rossby wave packets emanating from BHs to their geographical locations. This study also reveals that whether a BH over the eastern Pacific and Alaska can enhance or reduce the upward PW propagation is case-dependent. It is suggested that BHs that induce the stratospheric cooling can weaken statistical relationship between BHs and SSWs.

1. Introduction

It is well established that a stratospheric sudden warming (SSW), which is characterized by abrupt warming in the polar stratosphere, is induced by enhanced upward propagation of planetary waves (PWs) from the troposphere (Matsuno 1971). Many previous case studies on SSWs have pointed out that a tropospheric blocking high (BH), which gives rise to persistent anomalous meander of a tropospheric jet and abnormal weather conditions, can contribute to the enhancement of upward PW propagation that leads to the occurrence of an SSW event (e.g., Nishii et al. 2009). Quiroz (1986) found a statistical tendency of BHs to precede SSWs based on observational data for four winters. For a longer data period, this tendency has recently been confirmed by Martius et al. (2009), who demonstrated that BH frequency before SSWs tends to increase over ridges of the tropospheric climatological-mean PWs. Meanwhile, a few studies found BH development following SSW events (Labitzke 1965; Kodera and Chiba 1995; Mukougawa and Hirooka 2004). Taguchi (2008), however, could not find statistically significant changes in the frequency of BHs either before or after SSWs[1].

Recently, Orsolini et al. (2009) and Nishii et al. (2010), hereafter referred to as OKN09 and NNO10, respectively, observed a cooling tendency in the polar stratosphere

[1] Note that he used only BHs that induce amplification of tropospheric PWs. This will be discussed in section 6e.

following the BH development associated with the Western Pacific teleconnection pattern (Wallace and Gutzler 1981). They concluded that the cooling is contributed to by the suppression of upward PW propagation from the troposphere into the stratosphere, which is caused by the interference between the climatological-mean PWs and quasi-stationary circulation anomalies associated with an upward-propagating Rossby wave packet induced by the BH. Woollings et al. (2010) examined statistical relationships between dominant patterns of stratospheric variability, including the two types of SSWs (Charlton and Polvani 2007), and regional BH frequency. They suggested several different linkages between the stratospheric variability and BHs. They speculated that this diversity in the linkage may have made the SSW-BH issue controversial. As an example, they showed that stratospheric cooling can be induced through modulations of the stratospheric PWs by disturbances associated with BHs over the western North Pacific. Castanheira and Barriopedro (2010) also found a reduction in baroclinic energy of the zonal wavenumber 1 component (WN1) and the subsequent stratospheric vortex intensification in association with BHs over the North Pacific. This suppression of upward PW propagation has an implication that those BHs that induce stratospheric cooling, if included in the statistics, could involve some ambiguities into the statistical relationship between SSW events and BHs.

Before SSW events, BHs tends to be observed over permanent pressure ridges associated with the tropospheric climatological-mean PW (e.g., Martius et al. 2009), while BHs over the permanent troughs tend to suppress upward PW propagation (e.g., NNO10). This implies the importance of relative locations of BHs to the phase of the climatological-mean PW for the variability of upward PW propagation. The main aim of this study is to clarify the dependence of enhancement/suppression of upward PW propagation on the geographical position of BH development based on compositing of prominent BH events observed at every location over the extratropical Northern Hemisphere. The modulations of the upward PW propagations are studied quantitatively through the particular method formulated by Nishii et al. (2009) for analyzing the interference between the climatological-mean PWs and low-frequency circulation anomalies. The concept of the quasi-linear interference has recently regained attention in the studies of tropospheric influence on the stratospheric variability. Tropospheric circulation anomalies focused on in these studies include those associated with seesaw-like variability between Aleutian and Icelandic lows (Nakamura and Honda 2002), Rossby wave trains over Siberia (Takaya and Nakamura 2008; Kolstad and Charlton-Perez 2010; Smith et al. 2010), the Western Pacific teleconnection pattern (OKN09; NNO10), BHs (Martius et al. 2009; Nishii et al. 2009, 2010; Castanheira and Barriopedro 2010;

Woollings et al. 2010) and teleconnection from the tropics (Fletcher and Kushner 2011). We also identify preferred geographical locations of BH development that leads to extreme anomalies of the stratospheric polar vortex.

2. Data and analysis method

The Japanese 25-year Reanalysis (JRA-25; Onogi et al. 2007) is used for the period 1979-2008, available on a 2.5° x 2.5° latitude-longitudinal grid. In recognition of persistency of BHs, we focus on quasi-stationary circulation anomalies that have been extracted with a digital filter by retaining fluctuations with periods longer than 8 days in the original time series. Daily climatological-mean fields have been constructed for the period 1980-2007 based on 31-day running mean fields. Anomalies are defined locally as departures of the 8-day low-pass-filtered daily fields from the daily climatology for the corresponding calendar days.

Following Nakamura et al. (1997), we identified the 30 strongest BH events in winters (NDJFM) from 1979/1980 to 2007/2008, whose centers of the primary 250-hPa anticyclonic anomalies are within 500 km of a given reanalysis grid point. This identification of BHs was repeated for all other reanalysis grid points poleward of 30°N. See Appendix A for details. The particular number of events (30) has been chosen so that nearly one BH event is observed, on average, per season. The results shown below are

found qualitatively the same as those based on the 20 or 40 strongest BH events (not shown). For each of the grid points, the amplitude of the primary anticyclonic anomalies averaged over the 30 strongest BH events is substituted into the corresponding grid point in Fig. 1a. This map indicates that anticyclonic anomalies associated with BHs thus identified over the subpolar North Pacific tend to have largest amplitudes and secondarily over the subpolar North Atlantic. Anticyclonic anomalies are also strong over the Arctic region. The former two regions correspond well with the strongest variance and positive skewness of the 250-hPa height anomalies in winter (White 1980; Nakamura and Wallace 1991), which suggests that the high-amplitude anomalies over the two regions are largely contributed to by BHs.

Several different methods have been proposed for identifying BHs in instantaneous flow configurations with focus on potential vorticity or geopotential height (e.g., Barriopedro et al. 2006 and references therein). We nevertheless adopt our own method as described above, in recognition of the fact that circulation *anomalies* are more closely related to the activity of Rossby waves and their interference with the climatological-mean PWs. We have verified in Appendix B whether the anomaly events identified through our method are indeed BH events.

Circulation anomalies in the extratropical troposphere often develop in association

with Rossby wave-packet propagation. A typical example is wintertime BH development over Europe (Nakamura et al. 1997) or over Siberia (Takaya and Nakamura 2005ab), which is significantly contributed to by incoming horizontal Rossby wave packets. A wave-activity flux formulated by Takaya and Nakamura (2001) is suited for diagnosing three-dimensional propagation of localized Rossby wave packets through zonally-varying westerlies. In our evaluation of the flux, composited anomalies are regarded as fluctuations associated with Rossby waves, while the wintertime climatology (NDJFM) is used as the basic state. Hereafter, we simply call this flux a wave-activity flux.

Variability of upward PW propagation can be recognized as fluctuations in poleward eddy heat flux at the 100-hPa level averaged poleward of 45°N (Polvani and Waugh 2004; Nishii et al., 2009, 2010). From the 8-day low-pass-filtered fields of meridional wind velocity (V) and temperature (T), we estimated anomalous eddy heat flux $[V^*T^*]_a$, where the subscript a denotes an anomaly, the asterisks represent the zonally asymmetric component defined as deviations from their zonal means, and the square brackets signify the zonal and meridional averaging. Following Nishii et al. (2009), we then decomposed the 100-hPa $[V^*T^*]_a$ into individual contributions from $[V_a^*T_c^* + V_c^*T_a^*]$ and $[V_a^*T_a^*]_a$. Here, the subscript c denotes the daily climatological mean. The term

$[V_a{*}T_c{*} + V_c{*}T_a{*}]$ represents contributions from the interference between the climatological-mean PWs and anomalies, latter of which are often observed in association with upward-propagating Rossby wave packets (Nishii and Nakamura 2004, 2005; Nishii et al. 2009, 2010). The term $[V_a{*}T_a{*}]_a$ represents an anomalous instantaneous contribution from the anomalous wave packet propagation. If zonally averaged, the vertical component of the wave-activity flux formulated by Takaya and Nakamura (2001) is virtually equivalent to $[V_a{*}T_a{*}]$. Note that even if upward component of the wave-activity flux is observed, it does not necessarily contribute positively to $[V_a{*}T_a{*}]_a$ unless it is stronger than the climatology $[V_a{*}T_a{*}]_c$. Also note that even if $[V_a{*}T_a{*}]_a$ is small, Rossby wave packets may still cause significant stratospheric variability by modulating the climatological PWs through $[V_a{*}T_c{*} + V_c{*}T_a{*}]$. Similar diagnostic frameworks have been also adopted by Smith et al. (2010) and by Fletcher and Kushner (2011).

As discussed in Nishii et al. (2009) and Fletcher and Kushner (2011), part of the PW modulations can be discussed in terms of the interference, which is "linear" in a sense that it is a product of the climatological-mean PWs and quasi-stationary circulation anomalies. As elucidated in the evolution of potential vorticity (e.g., Takaya and Nakamura 2005b; OKN09; NNO10), amplification of BHs and their interaction with the climatological PW in the troposphere involve non-linear processes. Specifically, BHs

are often associated with potential vorticity breaking in the upper troposphere (Nakamura et al. 1997; Pelly and Hoskins 2003; see Appendix B for details). Feedback forcing from synoptic-scale eddies is also an essential factor for BH development around an oceanic stormtrack (e.g., Shutts 1983; Nakamura and Wallace 1993), which is another non-linear process.

Identification of 20 major SSW events by Tomikawa (2010) for winters from 1979/1980 to 2007/2008 based on the JRA-25 reanalysis data is utilized in this study. Those 20 events have been classified subjectively into the vortex displacement type (11 events) and vortex split type (9 event), in referring to the corresponding classification by Charlton and Polvani (2007) through an objective algorithm. The central dates of those events on which the 10-hPa zonal-mean zonal wind at 60°N turns into easterly are shown in Table 1. We have also identified extreme events of the Northern Annular mode (NAM), following Baldwin and Dunkerton (2001) but with a slightly modified definition. Specifically, the NAM pattern was identified as the first Empirical Orthogonal Function (EOF) of monthly-mean 10-hPa height anomalies in winter (NDJFM) over the domain poleward of 20°N. The daily NAM index was then calculated by projecting the low-pass-filtered daily 10-hPa height anomalies onto the NAM pattern. Fifteen events of the extremely strong polar vortex are listed in Table 1 for which the NAM in-

dex exceeds +2 standard deviations positively. The extremely strong vortex events are almost equivalent to the vortex intensification (VI) events identified by Limpasuvan et al. (2005).

3. Examples of composited BH evolution

In this section, results of our composite analysis are presented for distinctive BHs over the Barents Sea and the subpolar Far East (Fig. 1a). As shown later in Fig. 5a, the BHs in the former region are associated with enhanced upward PW propagation resulting in warming tendency of the polar stratosphere. In contrast, the BHs in the latter region lead to the suppression of the PW propagation giving rise to the anomalous cooling of the polar stratosphere.

a. BH over the Barents Sea (75°N, 42.5°E)

Composited evolution of temperature and geopotential height anomalies associated with BHs over the Barents Sea is shown in Fig. 2 (with the reference grid point indicated by a green dot). Five days before the peak time of the tropospheric BH (Fig. 2g), a Rossby wave train is observed across the Atlantic, which consists of anticyclonic anomalies over the U.S. east coast and the Barents Sea and of a cyclonic anomaly centered at the Labrador Strait. This wave train accompanies a well-defined northeastward

wave-activity flux. With this incoming wave-activity flux, the anticyclonic anomaly over the Barents Sea amplifies into a BH by the peak time (Fig. 2h). As the BH rapidly decays, another cyclonic anomaly develops over Siberia and Mongolia with an incoming wave-activity flux emanating from the BH upstream (Fig. 2i). The overall evolution is consistent with that for a BH over Europe as analyzed by Nakamura et al. (1997).

In the stratosphere, five days prior to the peak time of the BH (Fig. 2d), a pair of a cyclonic anomaly over the Labrador Strait and an anticyclonic anomaly over northern Eurasia appears to form a wave train with a well-defined eastward wave-activity flux. The flux diverges out of the cyclonic anomaly into which an upward wave-activity flux (blue contour in Fig. 2d) emanates from its tropospheric counterpart as a component of the tropospheric wave train across the Atlantic (Fig. 2g). The development of the stratospheric anticyclonic anomaly over Europe is also contributed to by an upward wave-activity flux over northern Europe (Fig. 2e). This stratospheric anomaly develops rapidly and persists over the Arctic region (Figs. 2e-f), giving rise to significant stratospheric warming through wave-mean flow interaction (Figs. 2b-c). The anomalous warm condition that prevails in the polar stratosphere persists even after the peak time of the BH (Fig. 2c) is evident in a composited time series of 50-hPa temperature anomaly averaged north of 70°N (purple line in Fig. 3a). This persistent warmth is associated

with enhanced upward PW propagation (positive $[V^*T^*]_a$; black), mainly through the interference terms ($[V_a^*T_c^* + V_c^*T_a^*]$; blue), but only slightly through the wave packet term ($[V_a^*T_a^*]_a$; red).

b. BH over the subpolar Far East (65°N, 167.5°E)

The next example shown in Fig. 4 highlights a BH over the subpolar Far East, which contributes to the cooling of the polar stratosphere by weakening the PWs. The evolution is quite similar to that of a blocking phase of the Western Pacific pattern shown by OKN09 and NNO10. In fact, an anticyclonic anomaly associated with the BH and a cyclonic anomaly to its south form a meridional dipole pattern in the troposphere that resembles the Western Pacific pattern (Fig. 4h). The anticyclonic anomaly develops in retrogressing from the central Pacific for several days before the peak time (Fig. 4g). The BH over the Far East develops under the strong feedback forcing from synoptic-scale eddies along the stormtrack (not shown). As it matures and then decays, the anticyclonic anomaly emits wave-activity flux downstream while forming a wave train over the North America (Figs. 4h-i). The wave train also emits the flux upward into the stratosphere (blue contours in Figs. 4e-f), which contributes to the development of a stratospheric wave train that consists of an anticyclonic anomaly over the Far East and a cyclonic anomaly over the North America (Figs. 4e-f). The cyclonic anomaly, which

accompanies a cool anomaly in the polar stratosphere five days after the peak time of the BH (Figs. 4c, 4f), persists for more than 10 days while gradually shifting poleward (not shown). This is consistent with a significant negative anomaly of the area-averaged polar stratospheric temperature after the peak time of the BH (purple line in Fig. 3b). This cooling can be explained by a significant reduction of $[V^*T^*]_a$ around the peak time, which is due solely to negative interference terms $[V_a^*T_c^* + V_c^*T_a^*]$ (blue line). The wave-packet term $[V_a^*T_a^*]_a$ (red line) is significantly positive, but not large enough to compensate the negative $[V_a^*T_c^* + V_c^*T_a^*]$.

4. Geographical dependence of the influence of BHs on the stratosphere

In this section, dependence is assessed of the anomalous upward PW propagation induced by BHs on their geographical locations over the Northern Hemisphere. We first constructed the composited time series similar to those shown in Fig. 3 for the 30 strongest anticyclonic anomaly events observed at each of the grid points over the extratropical Northern Hemisphere. As shown in Appendix B, most of these events are associated with BHs. For each of the variables, individual averages were then taken from lag +1 day to lag +10 day (labeled as period B in Fig. 3a), and finally the averaged value was assigned to the particular grid point where the BH events had been identified.

Figure 5a shows geographical distributions of the anomalous poleward heat flux associated with the entire PWs $[V^*T^*]_a$ that tends to be induced by BHs at individual geographical locations. Upward PW propagation tends to be enhanced with the maturity of BHs over North America, the North Atlantic, northern Europe and western Russia (yellow shading in Fig. 5a), while it tends to be suppressed with BHs that develop over the western Pacific and Far East (blue shading). Comparison between Figs. 5b and 5c reveals that the geographical dependency shown in Fig. 5a arises mainly from the contribution from WN1. Obviously, BHs developing over the climatological pressure ridge over the Euro-Atlantic sector and the trough over the western Pacific both associated with WN1 of the climatological-mean tropospheric PW tend to enhance and suppress upward propagation of WN1, respectively. Specifically, BH anomalies originating over the North Pacific tend to retrograde slowly over the zonally-elongated climatological-mean trough over the North Pacific and eastern Eurasia (Branstator 1987; Kushnir 1987; Takaya and Nakamura 2005b), yielding prolonged weakening of WN1 and associated upward PW propagation.

Decomposition of $[V^*T^*]_a$ as in Nishii et al. (2009) reveals that the anomalous $[V^*T^*]_a$ caused by BHs (Fig. 5a) over most of the regions over the Northern Hemisphere tends to be dominated by contributions from interference terms ($[V_a^*T_c^* +$

V_c*T_a*]; Fig. 5g) that represent modulations of the climatological-mean PWs by the BHs and associated anomalies. The dominant contribution from the interference terms is observed also in the anomalous upward propagation of WN1 and WN2 (Figs. 5b-c and 5h-i). These suggest that an upward-propagating wave packet from a BH, which is not necessarily one of the strongest, can effectively modulate the total PW fields and their propagation into the stratosphere.

In contrast, BH anomalies that develop over the eastern North Pacific and Alaska can induce no significant changes in the upward PW propagation (i.e., $[V^*T^*]_a \approx 0$ in Fig. 5a), as a consequence of the cancellation between a positive contribution from the wave-packet term (Fig. 5d) and a negative contribution from the interference terms (Fig. 5g). For those BHs, the interference term itself also includes partial cancellation between a dominant negative contribution from WN1 and a smaller positive contribution from WN2 (Figs. 5h-i). As will be discussed in section 6c, it is case-dependent for BHs over those two regions which contribution is dominant and thus whether the upward PW propagation is enhanced or suppressed.

In Fig. 6a, anomalous time tendency in the polar stratospheric temperature is assigned to a given location as an impact of the BH formation around that location that has been obtained from our composite analysis. The horizontal pattern of the temperature ten-

dency is quite similar to that of $[V^*T^*]_a$ shown in Fig. 5a. This similarity is understandable from a dynamical viewpoint where the intensity of stratospheric polar vortex can be changed by the modulated activity of the upward propagating PWs. At the same time, the similarity also confirms the substantial dependence of the modulations of the upward PW propagation and their influence on the stratospheric polar vortex upon the geographical location of a BH relative to the geographical phase of the climatological-mean PWs (Fig. 5a). Figure 6b indicates that a warm anomaly in the stratosphere tends to follow the maturity of BHs over northern or eastern Canada or over the Barents Sea, while the cool anomaly tends to be observed after the peak time of BHs over the western North Pacific or the Far East (OKN09; NNO10). In contrast to Fig. 6a, which shows anomalous temperature *tendency*, however, the signature of the polar stratospheric temperature *anomaly* itself (Fig. 6b) is less significant, especially over the Euro-Atlantic sector. This is because significant negative anomalies are observed in the polar stratospheric temperature even before the peak times of BHs over the subpolar Euro-Atlantic sector (not shown). It remains unclear, however, whether the stratospheric cool anomalies are favorable for triggering the tropospheric BH development over the Euro-Atlantic Sector and central Canada in any significant manner.

5. Geographical distribution of BHs as precursors of extreme stratospheric anom-

alies

Thus far, the sensitivity of stratospheric variability to BH locations has been investigated through composite analysis of BH events. Table 1 indicates, however, that occurrence of SSW events is much less frequent than that of tropospheric BHs, which suggests that some other factors should be involved in triggering the occurrence of those stratospheric events. It is thus instructive to identify preferred geographical locations of BHs that precede stratospheric extreme events. Red crosses in Fig. 7a and blue circles in Fig. 7b correspond to the anticyclonic anomaly centers of BHs observed in the periods prior to the major SSW events and the strong vortex events (Table 1), respectively. Obviously, the major SSW events tend to follow the maturity of BHs almost exclusively over North America, the North Atlantic and northern Europe, where $[V^*T^*]_a$ is positive associated with the BHs (yellow shading). The only exception is the eastern North Pacific, where $[V^*T^*]_a$ is nearly zero but with strongly positive $[V_a^*T_a^*]_a$ (Fig. 5d). In contrast, SSWs are quite unlikely to follow the maturity of BHs over the western North Pacific and Far East, which tend to yield negative $[V^*T^*]_a$ (blue shading).

The BH distribution associated with the SSWs shown in Fig. 7a is overall consistent with a map of composited 250-hPa height anomalies (Fig. 7e) prior to all the SSW events listed in Table 1. In the composite, anticyclonic anomalies are significant over

northwestern Canada and the North Atlantic. In those regions, the climatological-mean PW ridges are situated, and the PWs and their upward propagation can be intensified by the development of a BH (Fig. 5a). In contrast, the composited upper-tropospheric anomalies are cyclonic and collocated with the climatological-mean PW trough over the western North Pacific and Far East, which is consistent with the absence of BHs that lead to any of the major SSW events listed in Table 1. Rather, the strong vortex events listed in Table 1 follow the development of the BHs over the Far East, where $[V^*T^*]_a$ tends to be negative associated with the maturity of BHs (blue circles over light blue shading in Fig. 7a). This is again consistent with a composite map of 250-hPa anomalies prior to the strong vortex events in Table 1 (Fig. 7f), where a pronounced positive anomaly is found over the Far East. Over central Canada and the subpolar North Atlantic, BHs are not observed before the strong vortex events (Fig. 7b), where composited anomalies are cyclonic prior to the strong vortex events (Fig. 7f).

Martius et al. (2009) found that prior to SSWs of the vortex displacement type accompanied by the amplification of the stratospheric WN1, BH frequency tends to increase over the Euro-Atlantic sector. They also found that BH formation tends to be more frequent than in climatology over the central and eastern North Pacific and eastern North America prior to SSWs of the vortex split type that accompany the amplification

of both WN1 and WN2. Figures 7c and 7d indicate geographical locations at which BHs tend to be followed by SSW events of the vortex displacement type (green crosses) and split vortex type (purple circles), respectively. In good agreement with Fig. 1 of Martius et al. (2009), the displacement-type SSWs are likely to follow BH development mainly over the Euro-Atlantic sector, where BHs act to enhance WN1 propagation into the stratosphere (yellow shading) in Figs. 5b and 7c, but unlikely over the western Pacific and the Far East, where BHs act to suppress the upward WN1 propagation (blue shading in Fig 7c). In contrast, the split type of SSWs tends to follow BH formation over Alaska and northern Europe, which acts to amplify the upward WN2 propagation (yellow shading in Figs 5c and 7d)[2]. Some of these distinctions in the tropospheric precursors between the two types of SSWs are also seen in the composite anomaly fields of 250-hPa height in Figs. 7g-h. Even in the composite over all the major SSW events, for example, anticyclonic anomalies are significant over the North Atlantic for the vortex displacement type (Fig. 7g) and over North America for split vortex type (Fig. 7h). Another distinction is that the composited cyclonic anomalies over the North Pacific are shifted southeastward for the vortex displacement type compared to the split vortex type, which is consistent with more zonally-elongated PW trough over the Pacific with the

[2] The case dependency of BHs over Alaska in amplifying PWs will be discussed in section 6b.

stronger WN1 component.

6. Discussions

a. Connections of our findings to previous studies

Tropospheric circulation anomalies that are related to extreme stratospheric events have been identified in previous studies, and those anomalies are overall consistent with our findings. BHs over the Barents Sea discussed in section 3a may be related to an upper-tropospheric anticyclonic anomaly observed during the onset and growing stages of SSWs, as pointed out by Limpasuvan et al. (2004). Our composite analysis of tropospheric anomalies associated with the major SSW events (Fig. 7e) is consistent with that of Taguchi (2003), who found a tendency for tropospheric WN1 to amplify just before SSW events in an atmospheric model. Similar anomaly structures have been found by Garfinkel et al. (2010) in their composites for observed events of anomalously enhanced upward PW propagation and by Kolstad and Charlton-Perez (2010) in their composites for weak stratospheric polar vortex events in observations and climate models. The particular linkage of tropospheric circulation anomalies over the western North Pacific and Far East with strong vortex events as revealed in this study (e.g., Figs. 7b and 7f) is in good agreement with OKN09 and NNO10, and was already hinted in Limpasuvan et al.

(2005), Kolstad and Charlton-Perez (2010) and Orsolini et al. (2011).

In section 5, we have presented distribution of BHs that occur prior to the major SSW events (Fig. 7). A similar analysis was recently performed by Woollings et al. (2010; their Fig. 13). Comparison of their analysis with ours is, however, not necessarily straightforward, presumably because they focused on changes in the BH frequency associated with stratospheric variability.

b. Relative position of BHs to vertical waveguides for Rossby wave trains

Most of the BHs that modulate PW propagation, especially of the WN1, into the stratosphere, are located poleward of the latitude of the largest amplitude of the climatological-mean PWs (around 50°N; Fig. 5b), which may reflect the fact that the vertical waveguide for PWs into the stratosphere is located around 60°N (Karoly and Hoskins 1982). A particularly strong positive contribution to $[V_a{*}T_a{*}]_a$ from BHs over the eastern North Pacific (Fig. 5d) may arise from the tendency for anticyclonic anomalies associated with those BHs to attain the largest amplitudes (Fig. 1a), with their potential to act as strong sources of upward-propagating Rossby wave packets. It may also arise from the tendency for those wave packets to propagate upward effectively through a zonally-confined vertical waveguide that reflects the three-dimensional structure of the climatological-mean PWs (Nishii and Nakamura 2004; Nathan and Hodyss 2010).

c. Case sensitivity of BHs over Alaska (62.5°N, 215°E)

The composite analysis shown in Fig. 5a suggests that BHs over Alaska and the eastern Pacific, *as an ensemble*, do not modify upward PW propagation significantly. This is due to the cancelation between negative $[V^*T^*]_a$ by WN1 and positive $[V^*T^*]_a$ by WN2 both based on the composite analysis (Figs. 5b-c). Development of BHs over those two regions nevertheless tends to precede split-type SSW events (Fig. 7d). In fact, Harada et al. (2009) and Woollings et al. (2010) pointed out the importance of a BH signature over Alaska before a split-type SSW event in January 2009, to which the stratospheric WN2 contributed the most. Moreover, two events of Alaskan BH were consequently observed before a split-type SSW event in February 1989 (Table 1). An Alaskan BH developed, however, prior to a strong vortex event in late January 1984, suggesting that the influence of BHs on the stratosphere can vary qualitatively depending on individual BH events.

Out of the 30 strongest BH events observed around [62.5N, 215E] over Alaska, which are used for our composite analysis, we chose 10 events with the strongest positive $[V^*T^*]_a$ over the period (B) shown in Fig. 3a and another 10 events with the strongest negative $[V^*T^*]_a$. As shown in Figs. 8a-b, the composited BH anomaly for the 10 positive $[V^*T^*]_a$ events tends to remain over Alaska during the 5-day period after its

peak time. Staying over the climatological WN2 ridge, the BH can yield positive $[V_a{*}T_c{*} + V_c{*}T_a{*}]$ through WN2. This contribution is strong enough to dominate over the negative contribution from WN1 (Table 2), although the positive $[V_a{*}T_c{*} + V_c{*}T_a{*}]$, as a net, is not statistically significant over this period (blue line in Fig. 9a). In contrast, the composited BH anomaly for the 10 negative $[V{*}T{*}]_a$ events gradually retrogresses into the climatological-mean PW trough over the Far East (Fig. 8d). As exemplified in section 3b (Fig. 5b), a BH over this region tends to suppress the upward PW propagation. In addition, the BHs that yield negative $[V{*}T{*}]_a$ tend to accompany a cyclonic anomaly over the North Atlantic around its peak time, which also acts to weaken the climatological-mean tropospheric WN1 ridge (Fig. 8c). Reducing the positive $[V_a{*}T_c{*} + V_c{*}T_a{*}]$ by WN2, the retrogressive BH anomaly thus contributes strongly to the negative interference term by weakening WN1 (Table 2). This negative term retains its significance for about 15 days after the peak time (blue in Fig. 9b).

Another distinction between the two categories of the Alaskan BHs is found in the anomalous wave packet term $[V_a{*}T_a{*}]_a$. While nearly zero for those BHs with negative $[V{*}T{*}]_a$, this term is positive and even greater than the interference term $[V_a{*}T_c{*} + V_c{*}T_a{*}]$ for the BHs with positive $[V{*}T{*}]_a$, particularly after two or three days after the peak time (red in Fig. 9a), leading to the polar stratospheric warming (purple in Fig. 9a).

The enhanced upward wave-packet propagation that yields positive $[V_a{*}T_a{*}]_a$ tends to be observed over western Canada and the North Atlantic (not shown) along a local waveguide that connects the troposphere and stratosphere (Nakamura and Honda 2002). Due to the weak geographical coherency of the tropospheric anomalies downstream of those BHs, however, virtually no significant signature arises if composited (Fig. 8a).

A comparison between Figs. 8a and 8c reveals that the retrogressive BH anomaly tends to have somewhat greater zonal extent than the stationary BH anomaly. Further investigation is required on the causes of the two different types of time evolution of the Alaskan BH.

d. Modulations in vertical structure of PW by BHs

Upward-propagating Rossby waves accompany poleward eddy heat flux, exhibiting a westward phase tilt with height. Comparison of Figs. 4e and 4h, where the stratospheric anticyclonic anomaly is to the west of the tropospheric BH anomaly over the Far East, suggests that vertical phase lines of height *anomalies* tilt westward with height. This structure is similar to Fig. 2l of NNO10 and consistent with positive $[V_a{*}T_a{*}]_a$. Though less distinct, westward-tilting phase lines are observed in the composited height anomalies for the BHs over the Barents Sea (Figs. 2e and 2h). Nevertheless, vertical tilting of phase lines of the *entire* PW field (i.e., zonally asymmetric height field) differs qualita-

tively between those BHs. They are tilting westward with height for the BH over the Barents Sea, while virtually no tilting is observed in association with the BH over the Far East (not shown). These phase structures are consistent with the enhanced or suppressed $[V^*T^*]_a$ respectively.

The phase tilting can be inferred also from horizontal pattern correlation between meridional wind and temperature fields. The same composite maps as in Fig. 5a, but constructed for the pattern correlations between V^* and T^* (Fig. 10a) and between V_a^* and T_a^* (Fig. 10b) both over the domain poleward of 45°N at the 100-hPa level exhibit quite similar patterns to those of Figs. 5a and 5d, respectively. The positive V^*-T^* correlation tends to be enhanced by BHs over Canada and the Euro-Atlantic sector but reduced by BHs over the western North Pacific and Far East (Fig. 10a), whereas the positive V_a^*-T_a^* correlation tends to be increased only by BHs over the eastern North Pacific and Alaska (Fig. 10b). These results indicate that the enhancement or suppression of the entire PW and wave-packet propagation is largely a manifestation of changes in vertical phase structures of the PW and BH anomalies, respectively. They also indicate that the enhancement of the westward tilting of BH anomalies is not necessarily reflected in the entire PW structures.

e. SSWs and BHs

Taguchi (2008) could not find statistically significant relationship between SSWs and BHs. In his analysis, BHs that amplify the WN1 and/or 2 components of the tropospheric PWs by more than 25 m were taken into account. The BHs identified in our analysis either enhance or suppress the WN1 and 2 components of the tropospheric PWs, on average, by more than 50 m (not shown). One may wonder whether the inclusion of BHs that enhance PWs only modestly might reduce the statistical significance of the BH-SSW linkage as in the analysis by Taguchi (2008). However, BH events at each grid point analyzed in this study are observed, if any, at most only 2~3 times before the 20 SSW events listed in Table 1. The situation is qualitatively the same for the events of extremely strong vortex in Table 1. Our results suggest that most of BHs do not precede those extreme events, which may weaken the BH-SSW linkage in a statistical analysis. Nevertheless, as consistent with Martius et al. (2009), every major SSW event is preceded by the occurrence of BH(s) anywhere in the extratropical Northern Hemisphere, and so are most of the strong vortex events. Further investigation is required on the sufficient condition for the occurrence of extreme stratospheric events.

7. Conclusions

In the present study, a particular framework developed by Nishii et al. (2009) is ap-

plied to BH events observed all over the extratropical Northern Hemisphere, in order to quantify the contribution from the interference between Rossby wave packets propagating upward from BHs and the climatological-mean PWs to the anomalous upward PW propagation into the stratosphere. We also have assessed the relative importance between the particular interference and the wave-packet propagation in modulations of the upward PW propagation into the stratosphere. The importance of this interference has been pointed out and discussed qualitatively in some of the recent studies on BH influence on stratospheric variability (e.g., Martius et al. 2009; Woollings et al. 2010). Our analysis indicates that modulations of the three-dimensional structure of the PWs and the stratospheric polar vortex are sensitive to the BH location relative to the geographical phase of the climatological-mean tropospheric PW. We have revealed that tropospheric BHs around the pressure ridges of the tropospheric climatological-mean PWs over North America, the North Atlantic, Europe and western Russia tend to enhance upward PW propagation and thereby warm the polar stratosphere (Figs. 5 and 6). We have also revealed that BHs developing around a prominent PW trough over the western Pacific and the Far East tend to suppress the upward PW propagation and thereby cool the polar stratosphere. Weaker influence on the stratospheric temperature tends to be exerted, on average, by BHs developing over Alaska and the eastern North

Pacific, as their influence is case-sensitive. Specifically, a BH that is almost stationary tends to cause warming in the polar stratosphere, whereas a BH that slowly retrogresses towards the climatological-mean PW trough tends to cause the stratospheric cooling. We have also demonstrated that BHs over the western North Pacific and Far East are unlikely to give rise to SSWs but more likely to the intensification of the stratospheric polar vortex. We argue that the inclusion of those BHs that tend to induce stratospheric cooling may be one of the reasons for weak or no statistical linkage between SSWs and BHs analyzed in the previous studies. It should be pointed out that most of the BHs that enhance PW propagation into the stratosphere do not nevertheless precede any major SSWs. There must be some factors other than BH development for the occurrence of a major SSW event. The present study suggests that better representation of both the climatological-mean PWs and BH development at every geographical location in a forecast model may be necessary for the further improvement in the prediction of the stratospheric variability and its subsequent influence on the troposphere.

Acknowledgments

KN and HN are supported in part by the Japanese Ministry of Education, Culture, Sports, Science and Technology under the Grant-in-Aids for Scientific Research (B) 22340135 and on Innovative Areas 2205 and by the Japanese Ministry of Environment

under the Global Environment Research Fund (S-5). YO is supported by the Norwegian Research Council East Asian DecCen project (no 193690). The JRA-25 dataset is provided by the Japan Meteorological Agency and the Central Research Institute of Electric Power Industry. The Grid Analysis and Display System (GrADS) was used for drawing figures.

Appendix A. Identifying BH events

Our definition of a BH event is following Nakamura et al. (1997). For each of the re-analysis grid points ("a reference grid point"), the anticyclonic anomaly center in 250-hPa geopotential height observed within 500 km of that grid point was recorded every day over the 29 winter seasons (NDJFM). The 30 strongest events of the positive anomalies were then identified as BH events for the particular grid point. The peak time of a given BH event was defined as the day when the 250-hPa height anomaly at the BH center reached its minimum. This manipulation was repeated for all the grid points north of 30°N.

To construct Fig. 2 and Figs. 4-7, we composited the fields relative to the peak times of the 30 strongest anomaly events for a given reference grid point. First, the 250-hPa height anomaly fields at the peak times of the 30 events were composited without any other manipulations. The center of the composited anomaly was regarded as a “target” anomaly center. The entire fields for the individual events were then shifted slightly before being composited. The shifting was performed in such a manner that the strongest anticyclonic anomaly in 250-hPa height for each of the events coincided with the “target” anomaly center. This shifting was performed by rotating each of the fields along a great circle that connects the prescribed “target” anomaly center and the primary

250-hPa anomaly center at the peak time of a particular event. This translation should not lead to any serious loss of geographical identities of the composited signatures, since the shifting was less than 500 km, i.e., substantially less than the horizontal scale of a BH. This translation was applied in order to retain the sharpness of the composited signatures. For each of the BH events observed around a given reference grid point, the same translation was applied to all variables for all time-lags relative to the peak time of the event. As can be seen in the composited maps, the composited 250-hPa height anomaly center at the peak time does not necessarily coincide with the reference grid point. For constructing the composited time series plotted in Fig. 3, a time series of a given variable had been obtained for each of the BH events, which was then composited relative to the peak time.

Appendix B. Comparison with other definitions of BHs

As explained in Appendix A, our identification of a BH event is based on amplitudes of low-pass-filtered height anomalies, and therefore our events may have to be called "high-amplitude persistent anomaly events" (cf., Dole and Gordon 1983). In this appendix, those events identified in this study are checked whether they really have characteristics of BHs. A distinctive characteristic of a BH is local weakening and splitting of the westerlies. Sumner (1954) focused on a cutoff anticyclonic flow configuration in 500-hPa height and sea-level pressure fields as characteristics of a BH. The particular flow configuration is associated with a local maximum in the total height (or pressure) field surrounded by closed contours, with the local easterlies to the south of the maximum. In this study, we only use 500-hPa height fields for identifying cutoff anticyclones. For each of the high-amplitude anomaly events identified around a given reference grid point, we checked whether the anomaly accompanies a positive local maximum in the 8-day low-pass-filtered 500-hPa total height field within 1500 km of the reference grid point in the three-day period centered at the peak time of a particular event (lags of 0 and ± 1 days). Figure 1b shows the percentages of our high-amplitude anticyclonic anomaly events that accompany a cutoff-high configuration for the individual reference grid points. Most of our events over the North Atlantic, northern Eu-

rope, the subpolar Far East and the eastern North Pacific are found to accompany cutoff anticyclones. In contrast, cutoff anticyclones are less likely to be observed in association with anomaly events over the mid-latitude regions from the Mediterranean to the western North Pacific and over the eastern portion of North America, where the anticyclonic anomalies are unlikely to attain particularly large amplitudes (Fig. 1a).

Persistent large-scale Rossby wave breaking at the tropopause level is another essential aspect of BHs (Nakamura et al 1997; Pelly and Hoskins 2003; Woollings et al. 2008). In our analysis, the breaking was identified as the reversal of the local meridional gradient of a potential temperature on the surface of 2 potential vorticity (PV) unit by comparing area-averaged potential temperature between a pair of meridionally adjacent boxes in size of 5° in longitude and 15° in latitude (see Fig. 2 of Pelly and Hoskins 2003 for a schematic diagram). For a given anomaly event, the breaking signature was searched within 2000 km of the primary anticyclonic anomaly center at the peak day, and we recorded persistent breaking events that had been observed consecutively over 5 days or longer around the peak time. For a technical reason, the occurrence of breaking was checked only for anomaly events observed between 40°N and 75°N. As shown in Fig. 1c, most of the anomaly events (over 90%) in mid- and high latitudes accompany wave breaking. Figures 1b and 1c suggest that in most of the polar and subpolar regions

over the Northern Hemisphere, the large-amplitude anticyclonic anomaly events identified in our analysis exhibit the characteristics of BHs. The only exception is central and eastern Canada. Nevertheless, the majority of the events still exhibit the characteristics of BHs.

References

Baldwin, M. P., and T. J. Dunkerton, 2001: Stratospheric harbinger of anomalous weather regimes. *Science*, **294**, 581– 584.

Barriopedro, D., R. García-Herrera, A. R. Lupo, and E. Hernández, 2006: A climatology of Northern Hemisphere blocking. *J. Climate*, **19**, 1042-1063.

Branstator, G. 1987: A striking example of the atmosphere's leading traveling pattern. *J. Atmos. Sci.,* **44**, 2310-2323.

Castanheira, J. M., and D. Barriopedro, 2010: Dynamical connection between tropospheric blockings and stratospheric polar vortex. *Geophys. Res. Lett.*, **37**, L13809, doi:10.1029/2010GL043819.

Charlton, A. J., and L. M. Polvani, 2007: A new look at stratospheric sudden warmings. Part I: Climatology and modeling benchmarks. *J. Climate,* **20***,* 449-469.

Cheng, X., and T. J. Dunkerton, 1995: Orthogonal rotation of spatial patterns derived from singular value decomposition analysis. *J. Climate.,* **8**, 2631-2643.

Dole, R. M., and N. D. Gordon, 1983: Persistent anomalies of the extratropical Northern Hemisphere wintertime circulation: Geographical distribution and regional persistence characteristics. *Mon., Wea., Rev.*, **111**, 1567-1586.

Fletcher C. G., and P. J. Kushner, 2011: The role of linear interference in the annular

mode response to tropical SST forcing. *J. Climate,* **24**, 778-794.

Garfinkel, C. I., D. L. Hartmann, and F. Sassi, 2010: Tropospheric precursors of anomalous Northern Hemisphere stratospheric polar vortices. *J. Climate*, **23***,* 3282-3299, doi: 10.1175/2010JCLI3010.1.

Harada Y., A. Goto, H. Hasegawa, H. Naoe, and T. Hirooka, 2009: A major stratospheric sudden warming event in January 2009. *J. Atmos. Sci.,* **67**, 2052–2069.

Karoly, D. J., and B. J. Hoskins, 1982: Three dimensional propagation of planetary waves. *J. Meteor. Soc. Japan,* **60***,* 109-123.

Kodera, K., and M. Chiba, 1995: Tropospheric circulation changes associated with stratospheric sudden warmings: A case study. *J. Geophys. Res.,* **100***,* 11055-11068.

Kolstad, E. W., and A. Charlton-Perez, 2010: Observed and simulated precursors of stratospheric polar vortex anomalies in the Northern Hemisphere. *Climate Dyn.*, *in press,* DOI: 10.1007/s00382-010-0919-7

Kushnir, Y., 1987: Retrograding wintertime low-frequency disturbances over the North Pacific Ocean. *J. Atmos. Sci.,* **44***,* 2727-2742.

Labitzke, K., 1965: On the mutual relation between stratosphere and troposphere during periods of stratospheric warmings in winter. *J. Appl. Meteor.,* **4***,* 91-99.

Limpasuvan V., D. W. J. Thompson, and D. L. Hartmann, 2004: The life cycle of the Northern Hemisphere sudden stratospheric warmings. *J. Climate,* **17**, 2584-2596.

Limpasuvan V., D. L. Hartmann, D. W. J. Thompson, K. Jeev, and Y. L. Yung, 2005: Stratosphere-troposphere evolution during polar vortex intensification. *J. Geophys. Res.,* **110**, D24101, doi:10.1029/2005JD006302.

Martius, O., L. M. Polvani, and H. C. Davies, 2009: Blocking precursors to stratospheric sudden warming events. *Geophys. Res. Lett.,* **36***,* L14806, doi:10.1029/2009GL038776.

Masuno, T., 1971: A dynamical model of stratospheric sudden warming. *J. Atmos. Sci.,* **28***,* 1479-1494.

Mukougawa, H., and T. Hirooka, 2004: Predictability of stratospheric sudden warming: A case study for 1998/99 Winter. *Mon. Wea. Rev.,* **132***,* 1764-1776.

Nakamura, H., and J. M. Wallace, 1991: On the skewness of low-frequency fluctuations in the tropospheric circulation during the Northern Hemisphere winter. *J. Atmos. Sci.,* **48**, 1441-1448.

Nakamura, H., and J. M. Wallace, 1993: Synoptic behavior of baroclinic eddies during the blocking onset. *Mon. Wea. Rev.*, **121**, 1892-1903.

Nakamura, H., M. Nakamura, and J. L. Anderson, 1997: The role of high- and low-frequency dynamics in blocking formation. *Mon. Wea. Rev.,* **125***,* 2074-2093.

Nakamura , H., and M. Honda, 2002: Interannual seesaw between the Aleutian and Icelandic lows. Part III: Its influence upon the stratospheric variability. *J. Meteor. Soc. Japan,* **80***,* 1051-1067.

Nathan, T. R., and D. Hodyss, 2010: Troposphere–stratosphere communication through local vertical waveguides. *Quart. J. Roy. Meteor. Soc.,* **136**, 12-19.

Nishii, K., and H. Nakamura, 2004: Lower-stratospheric Rossby wave trains in the Southern Hemisphere: A case study for late winter of 1997. *Quart. J. Roy. Meteor. Soc.,* **130***,* 325-345.

Nishii, K., and H. Nakamura, 2005: Upward and downward injection of Rossby wave activity across the tropopause: A new aspect of the troposphere-stratosphere dynamical linkage. *Quart. J. Roy. Meteor. Soc.,* **131***,* 39-52.

Nishii, K., H. Nakamura, and T. Miyasaka, 2009: Modulations in the planetary wave field induced by upward-propagating Rossby wave packets prior to stratospheric sudden warming events: A case study. *Quart. J. Roy. Meteor. Soc.,* **135***,* 39-52.

Nishii, K., H. Nakamura, and Y. J. Orsolini, 2010: Cooling of the wintertime Arctic

stratosphere induced by the Western Pacific teleconnection pattern. *Geophys. Res. Ltt.,* **37***,* L13805, doi:10.1029/2010GL043551.

Onogi, K., et al., 2007: The JRA-25 reanalysis. *J. Meteor. Soc. Japan.,* **85***,* 369-432.

Orsolini, Y. J., A. Y. Karpechko, and G. Nikulin, 2009: Variability of the Northern Hemisphere polar stratospheric cloud potential: The role of North Pacific disturbances. *Quart. J. Roy. Meteor. Soc.,* **135**, 1020-1029.

Orsolini, Y. J., I. T. Kindem, N. G. Kvamstø, 2011: On the potential impact of the stratosphere upon seasonal dynamical hindcasts of the North Atlantic Oscillation: a pilot study. *Climate Dyn.*, **36**, 579-588.

Pelly, J. L., and B. J. Hoskins, 2003: A new perspective on blocking. *J. Atmos. Sci.,* **60***,* 743-755.

Polvani, L. M., and D. W. Waugh, 2004: Upward wave activity flux as a precursor to extreme stratospheric events and subsequent anomalous surface weather regimes. *J. Climate*, **17**, 3548-3554.

Quiroz, R. S., 1986: The association of stratospheric warmings with tropospheric blocking. *J. Geophys. Res.,* **91***,* 5277-5285.

Shutts, G. J., 1983: The propagation of eddies in diffluent jetstreams: Eddy vorticity

forcing of blocking flow fields, *Quart. J. Roy. Meteor. Soc.,* **109**, 737-761.

Smith, K. L., C. G. Fletcher, and P. J. Kushner, 2010: The role of linear interference in the Annular mode response to extratropical surface forcing. *J. Clim*ate, **23**, 6036-6050.

Sumner, E. J., 1954: A study of blocking in the Atlantic-European sector of the Northern Hemisphere. *Quart. J. Roy. Meteor. Soc.*, **80**, 402-416.

Takaya, K., and H. Nakamura, 2001: A formulation of a phase-independent wave-activity flux of stationary and migratory quasi-geostrophic eddies on a zonally varying basic flow. *J. Atmos. Sci.,* **58***,* 608-627.

Takaya, K., and H. Nakamura, 2005a: Mechanisms of intraseasonal amplification of the cold Siberian High. *J. Atmos. Sci.*, **62**, 4423-4440.

Takaya, K., and H. Nakamura, 2005b: Geographical dependence of upper-level blocking formation associated with intraseasonal amplification of the Siberian High. *J. Atmos. Sci*., **62**, 4441-4449.

Takaya, K., and H. Nakamura, 2008: Precursory changes in planetary wave activity for midwinter surface pressure anomalies over the Arctic. *J. Meteor. Soc. Japan*, **86**, 415-427.

Taguchi, M., 2003: Tropospheric response to stratospheric sudden warmings in a simple global circulation model. *J. Climate*, **16**, 3039-3049.

Taguchi, M., 2008: Is there a statistical connection between stratospheric sudden warming and tropospheric blocking events? *J. Atmos. Sci.,* **65***,* 1442-1454.

Tomikawa, Y., 2011: Persistence of easterly wind during major stratospheric sudden warmings, *J. Climate,* **23**, 5258-5267.

Wallace, J. M., and D. S. Gutzler, 1981: Teleconnections in the geopotential height field during the Northern Hemisphere winter. *Mon. Wea. Rev.,* **109***,* 784-812.

White, G. H., 1980: Skewness, kurtosis and extreme values of northern hemisphere geopotential heights. *Mon. Wea. Rev.,* **108**, 1446-1455.

Woollings, T. A., B. Hoskins, M. Blackburn, and P. Berrisford, 2008: A new Rossby wave-breaking interpretation of the North Atlantic Oscillation. *J. Atmos. Sci.,* **65***,* 609-626, doi:10.1175/2007JAS2347.1.

Woollings, T., A. J. Charlton-Perez, S. Ineson, A. G. Marshall, and G. Masato, 2010: Associations between stratospheric variability and tropospheric blocking. *J. Geophys. Res.,* **115***,* D06108, doi:10.1029/2009JD012742.

Table 1. Central dates of major SSW events of the vortex displacement type and vortex split type and of the events of the extremely strong vortex for the Northern Hemisphere.

Vortex displacement type SSW (11 events)	Vortex split type SSW (9 events)	Extremely strong vortex (15 events)
29 February 1980	1 January 1985	29 December 1980
6 February 1981	8 December 1987	8 February 1980
4 December 1981	14 March 1988	11 January 1983
24 February 1984	21 February 1989	31 January 1984
23 January 1987	15 December 1998	26 February 1986
20 March 2000	26 February 1999	13 February 1988
31 December 2001	11 February 2001	19 January 1989
21 January 2006	18 January 2003	7 January 1990
24 February 2007	7 January 2004	28 January 1993
22 February 2008		2 March 1994
14 March 2008		12 March 1995
		7 February 1996
		25 March 1997
		10 January 2000
		11 February 2005

Table 2. Poleward eddy heat fluxes composited separately for the two categories of BH events over Alaska (62.5N, 215E), 10 events with strongest positive $[V^*T^*]_a$ (upper) averaged over the period (B) in Fig. 3a, and another 10 events with strongest negative $[V^*T^*]_a$. (lower).

	$[VT]_a$	$[V_aT_a]_a$	$[V_aT_c+V_cT_a]$	$[V_aT_c+V_cT_a]$(WN1)	$[V_aT_c+V_cT_a]$(WN2)
Positive $[VT]_a$	7.8	5.4	2.4	-3.5	5.8
Negative $[VT]_a$	-7.1	0.9	-8.1	-9.8	1.0

Figure captions

Figure 1. (a) Distribution of the mean amplitude of the primary anomaly in 250-hPa height for the 30 strongest anticyclonic events ("BH" events) observed around a given grid point (shading: m), superimposed on the zonally asymmetric component of the 250-hPa climatological-mean height in winter (contour; unit: m). (b) Fraction (%) of BH events that accompany cutoff anticyclones out of the 30 events observed around a given location. See Appendix B for details. (c) As in (b) but for the fraction of BH events that accompany Rossby wave breaking. The occurrence of the breaking was not checked where shading is not applied.

Figure 2. (a) Anomaly fields (black lines for every 2K; dashed for negative; no zero lines) of 50-hPa temperature composited for 5 days before the peak time of the 30 BH events observed around the Barents Sea (75°N, 42.5°E; denoted by a green dot). Significant positive and negative anomalies in 50-hPa temperature at the 95% confidence level based on the t-statistic are indicated with yellow and light blue shading, respectively. (b-c) Same as in (a), but for (b) the peak times of the BH events and (c) 5 days after the peak times. (d-f) Same as in (a-c), respectively, but for the composited 30-hPa height anomaly of 30-hPa height (black lines for every 50 m; dashed for negative; zero lines

omitted). Horizontal component of the wave-activity flux based on the composited anomalies at the 30-hPa level is indicated by red arrows (with the reference magnitude (m^2 s^{-2}) at the bottom of (f). Upward component of the corresponding flux across the 100-hPa level exceeds 0.001 $m^2 s^{-2}$ in the region surrounded by heavy blue lines. (g-i) Same as in (d-f), respectively, but for 250-hPa height anomaly.. The reference magnitude of the horizontal component of 250-hPa wave-activity flux is at the bottom of (i).

Figure 3. (a) Composited time series for the 30 BH events over the Barents Sea (75°N, 42.5°E). Black, red and blue lines indicate $[V^*T^*]_a$, $[V_a^*T_a^*]_a$ and $[V_a^*T_c^* + V_c^*T_a^*]$ at the 100-hPa level averaged poleward of 45°N (left axis: K m s^{-1}), respectively, and a purple line represents 50-hPa temperature anomaly averaged poleward of 70°N (right axis: K). Anomalies that are significant at the 95% confidence level are highlighted with dots. Arrows and labels show periods for (A) lag -10 to -1 days, (B) lag +1 to +10 days, (C) lag +11 to +20 days of the peak time. (b) Same as (a), but for the subpolar Fat East (65°N, 167.5°E).

Figure 4. Same as in Fig. 2, but for 30 BH events over the subpolar Far East (65°N, 167.5°E).

Figure 5. (a) Area-averaged $[V^*T^*]_a$ poleward of 45°N averaged over the period (B) (shown in Fig. 3a) composited for the 30 BH events observed around a given location. Contour interval is 2 K m s^{-1} (black lines; dashed for negative; zero lines omitted). Significant positive (negative) values of $[V^*T^*]_a$ at the 95 % confidence level based on the *t*-statistic are indicated by yellow (blue) shading. See text for details. Red contours are for deviations of climatological-mean 250-hPa geopotential height from its zonal mean (solid for 100 m; dashed for -100 m). (b-c) Same as in (a), but for $[V^*T^*]_a$ associated only with (b) WN1 and (c) WN2, respectively. Red contours indicate the climatological-mean 250-hPa geopotential height (solid for 100 m; dashed for -100 m) associated only with (b) WN1 and (c) WN2. (d) Same as in (a), but for the interference term ($[V_a^*T_c^* + V_c^*T_a^*]$). (e-f) Same as in (d), but for the wave-packet term $[V_a^*T_a^*]_a$ associated only with (e) WN1 and (f) WN2. In each of panels, dots denote the centers of BHs exemplified in section 3.

Figure 6. (a) Same as in Fig. 3a, but for anomalous time tendency in composited 50-hPa temperature (contoured for every 2K) poleward of 70°N, as inferred as the difference between the two periods (C) and (A) shown in Fig. 3a. Dark (light) shading de-

notes significant positive (negative) tendency at the 95 % confidence level based on the t-statistic. (b) Same as in (a), but for the composited 50-hPa temperature anomaly averaged over the period (C) as shown in Fig. 3a.

Figure 7. (a) Red crosses denote grid points where BHs are observed within the period between lags -10 and -1 days relative to the central days of the major SSW events. The shading is the same as in Fig. 5a, but positive and negative anomalies are represented with yellow and blue shading, respectively. (b) Blue circles denote BHs detected within the period between lags -10 and -1 days relative to the peak days of the strong vortex events. (c) Green crosses are for BHs detected within the period between lags -10 and -1 days relative to the central days of the displacement type SSWs. The shading is the same as in Fig. 5b. (d) As in (c), but for the split type SSWs (purple circles). The shading is the same as in Fig. 5c. (e) Map of 250-hPa geopotential height anomaly composed for the all the major SSW events listed in Table 1, based on averages over the period -10 days to -1 day relative to the the central dates of the SSWs. Contour interval is 50 m (dashed for negative; zero lines omitted). Heavy contours represent total 250-hPa height (9800 and 10200 m). (f-h) Same as in (e), but for the (f) strong vortex events, (g) displacement-type SSWs and (h) split-type SSWs, respectively, as listed in Table 1.

Figure 8. (a) Same as in Fig. 2h, but for 10 BH events over Alaska (62.5°N, 215°E) that accompany strongest positive $[V^*T^*]_a$. (b) Same as in (a), but for the lag of +5 day. (c) Same as in (a), but for another 10 BH events that accompanies strongest negative $[V^*T^*]_a$. (d) Same as in (c), but for the lag +5 day.

Figure 9. (a) As in Fig. 3a, but for 10 BH events over Alaska (62.5°N, 215°E) that accompany strongest positive $[V^*T^*]_a$. (b) As in (a), but for another 10 BH events that accompany strongest negative $[V^*T^*]_a$.

Figure 10. (a) As in Fig. 5a, but for composited anomalies for the pattern correlation between V^* and T^* over the domain poleward of 45°N at the 100-hPa level. (b) As in (a), but for pattern correlation between V_a^* and T_a^*.

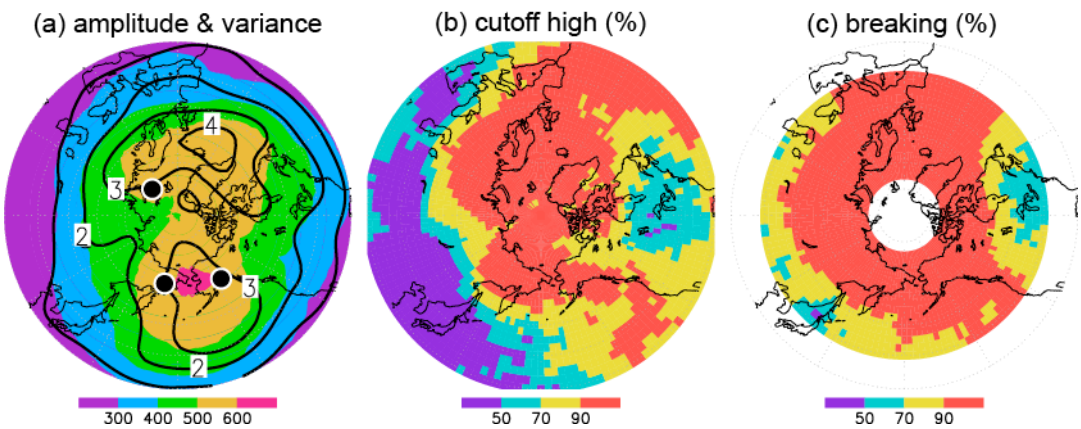

Figure 1. (a) Distribution of the mean amplitude of the primary anomaly in 250-hPa height for the 30 strongest anticyclonic events ("BH" events) observed around a given grid point (shading: m), superimposed on the zonally asymmetric component of the 250-hPa climatological-mean height in winter (contour; unit: m). (b) Fraction (%) of

BH events that accompany cutoff anticyclones out of the 30 events observed around a given location. See Appendix B for details. (c) As in (b) but for the fraction of BH events that accompany Rossby wave breaking. The occurrence of the breaking was not checked where shading is not applied.

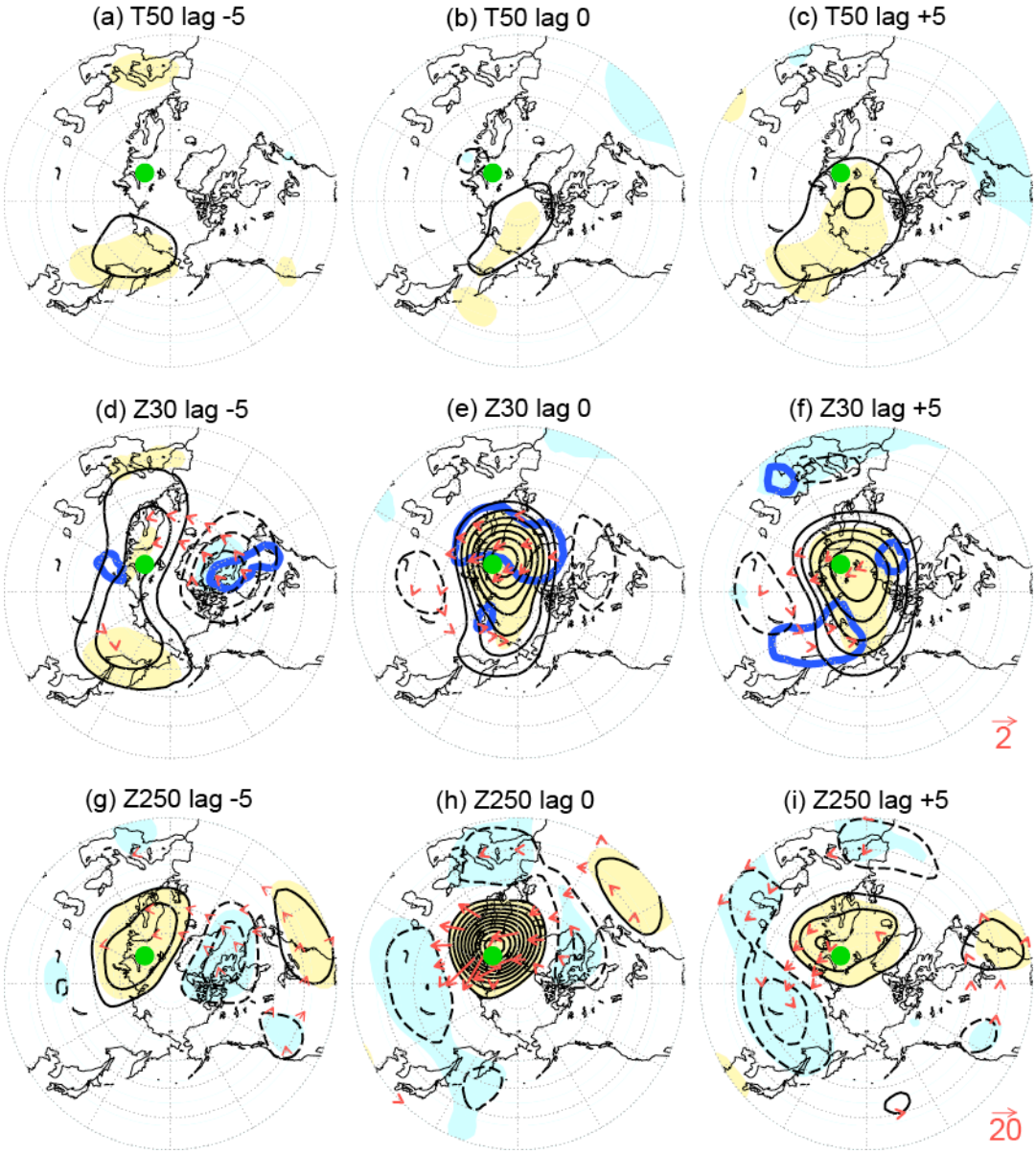

Figure 2. (a) Anomaly fields (black lines for every 2K; dashed for negative; no zero lines) of 50-hPa temperature composited for 5 days before the peak time of the 30 BH

events observed around the Barents Sea (75°N, 42.5°E; denoted by a green dot). Significant positive and negative anomalies in 50-hPa temperature at the 95% confidence level based on the t-statistic are indicated with yellow and light blue shading, respectively. (b-c) Same as in (a), but for (b) the peak times of the BH events and (c) 5 days after the peak times. (d-f) Same as in (a-c), respectively, but for the composited 30-hPa height anomaly of 30-hPa height (black lines for every 50 m; dashed for negative; zero lines omitted). Horizontal component of the wave-activity flux based on the composited anomalies at the 30-hPa level is indicated by red arrows (with the reference magnitude (m^2 s^{-2}) at the bottom of (f). Upward component of the corresponding flux across the 100-hPa level exceeds 0.001 $m^2 s^{-2}$ in the region surrounded by heavy blue lines. (g-i) Same as in (d-f), respectively, but for 250-hPa height anomaly.. The reference magnitude of the horizontal component of 250-hPa wave-activity flux is at the bottom of (i).

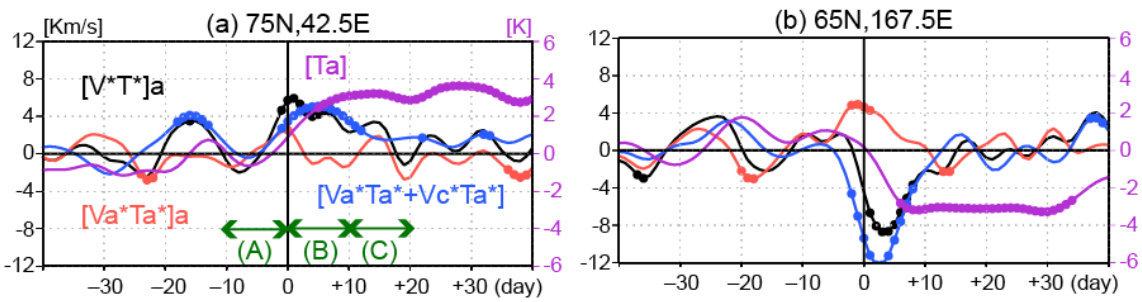

Figure 3. (a) Composited time series for the 30 BH events over the Barents Sea (75°N, 42.5°E). Black, red and blue lines indicate $[V^*T^*]_a$, $[V_a^*T_a^*]_a$ and $[V_a^*T_c^* + V_c^*T_a^*]$ at the 100-hPa level averaged poleward of 45°N (left axis: K m s^{-1}), respectively, and a purple line represents 50-hPa temperature anomaly averaged poleward of 70°N (right axis: K). Anomalies that are significant at the 95% confidence level are highlighted with dots. Arrows and labels show periods for (A) lag -10 to -1 days, (B) lag +1 to +10 days, (C) lag +11 to +20 days of the peak time. (b) Same as (a), but for the subpolar Fat East (65°N, 167.5°E).

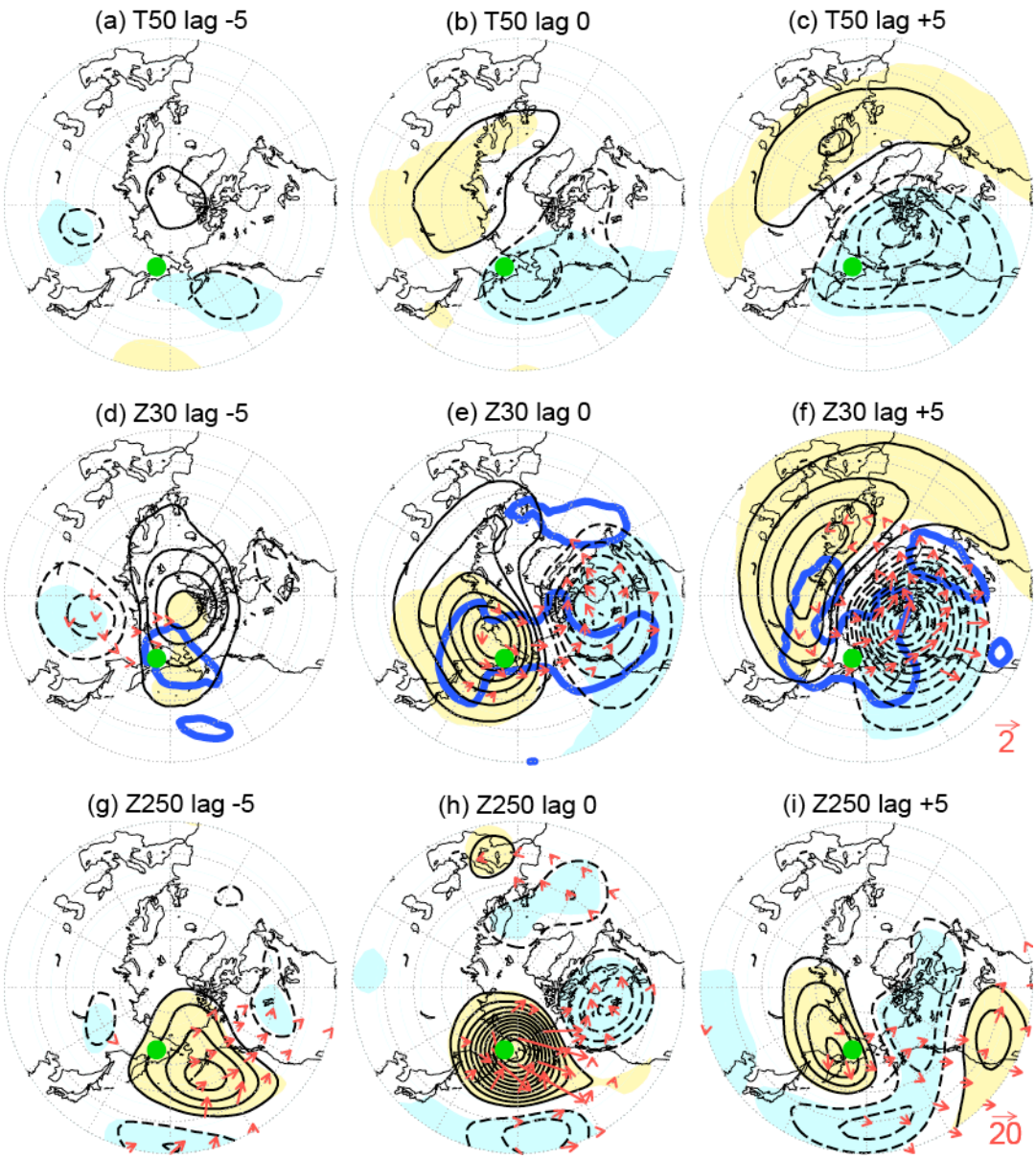

Figure 4. Same as in Fig. 2, but for 30 BH events over the subpolar Far East (65°N, 167.5°E).

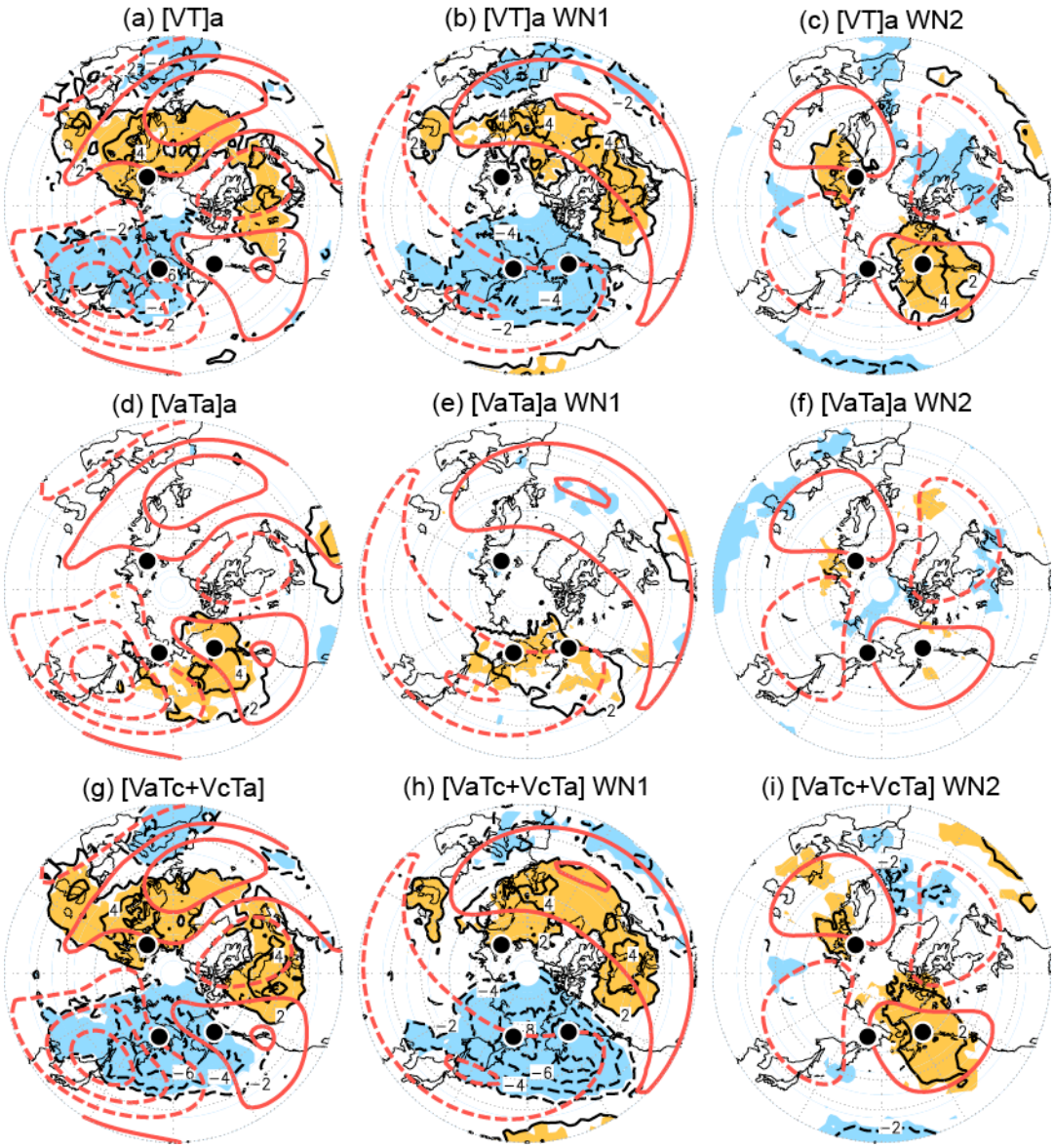

Figure 5. (a) Area-averaged $[V^*T^*]_a$ poleward of 45°N averaged over the period (B) (shown in Fig. 3a) composited for the 30 BH events observed around a given location. Contour interval is 2 K m s^{-1} (black lines; dashed for negative; zero lines omitted). Significant positive (negative) values of $[V^*T^*]_a$ at the 95 % confidence level based on the *t*-statistic are indicated by yellow (blue) shading. See text for details. Red contours are for deviations of climatological-mean 250-hPa geopotential height from its zonal mean

(solid for 100 m; dashed for -100 m). (b-c) Same as in (a), but for $[V^*T^*]_a$ associated only with (b) WN1 and (c) WN2, respectively. Red contours indicate the climatological-mean 250-hPa geopotential height (solid for 100 m; dashed for -100 m) associated only with (b) WN1 and (c) WN2. (d) Same as in (a), but for the interference term ($[V_a^*T_c^* + V_c^*T_a^*]$). (e-f) Same as in (d), but for the wave-packet term $[V_a^*T_a^*]_a$ associated only with (e) WN1 and (f) WN2. In each of panels, dots denote the centers of BHs exemplified in section 3.

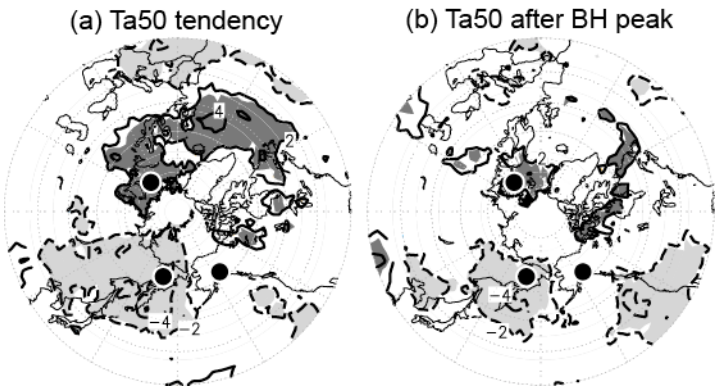

Figure 6. (a) Same as in Fig. 3a, but for anomalous time tendency in composited 50-hPa temperature (contoured for every 2K) poleward of 70°N, as inferred as the difference between the two periods (C) and (A) shown in Fig. 3a. Dark (light) shading denotes significant positive (negative) tendency at the 95 % confidence level based on the t-statistic. (b) Same as in (a), but for the composited 50-hPa temperature anomaly averaged over the period (C) as shown in Fig. 3a.

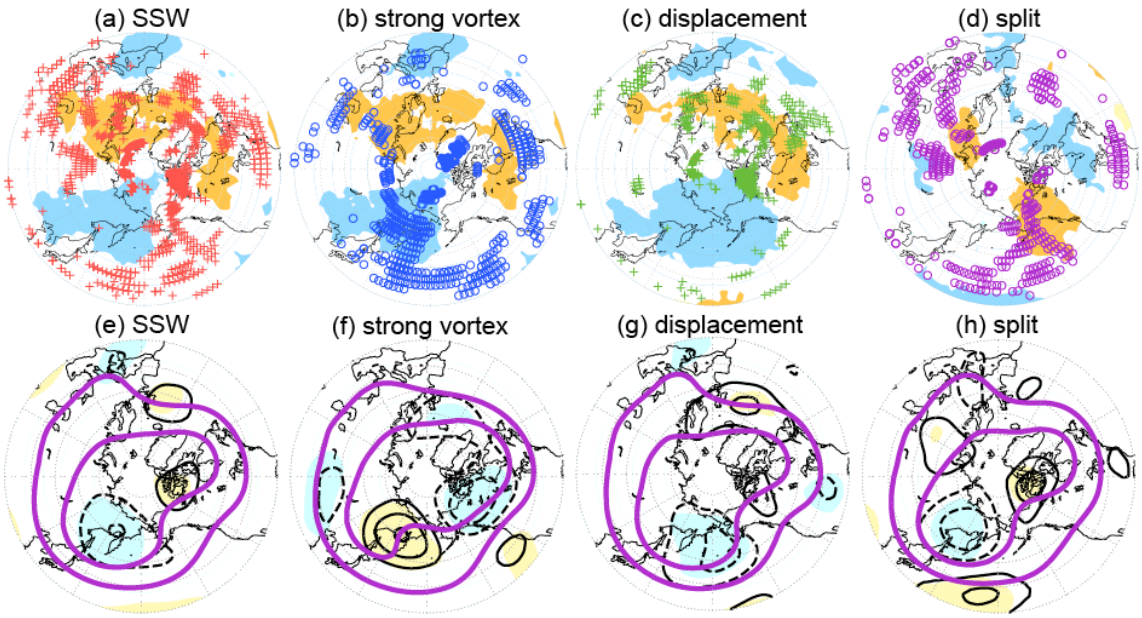

Figure 7. (a) Red crosses denote grid points where BHs are observed within the period between lags -10 and -1 days relative to the central days of the major SSW events. The shading is the same as in Fig. 5a, but positive and negative anomalies are represented with yellow and blue shading, respectively. (b) Blue circles denote BHs detected within the period between lags -10 and -1 days relative to the peak days of the strong vortex events. (c) Green crosses are for BHs detected within the period between lags -10 and -1 days relative to the central days of the displacement type SSWs. The shading is the same as in Fig. 5b. (d) As in (c), but for the split type SSWs (purple circles). The shading is the same as in Fig. 5c. (e) Map of 250-hPa geopotential height anomaly composed for the all the major SSW events listed in Table 1, based on averages over the period -10 days to -1 day relative to the the central dates of the SSWs. Contour interval is 50 m (dashed for negative; zero lines omitted). Heavy contours represent total 250-hPa height

(9800 and 10200 m). (f-h) Same as in (e), but for the (f) strong vortex events, (g) displacement-type SSWs and (h) split-type SSWs, respectively, as listed in Table 1.

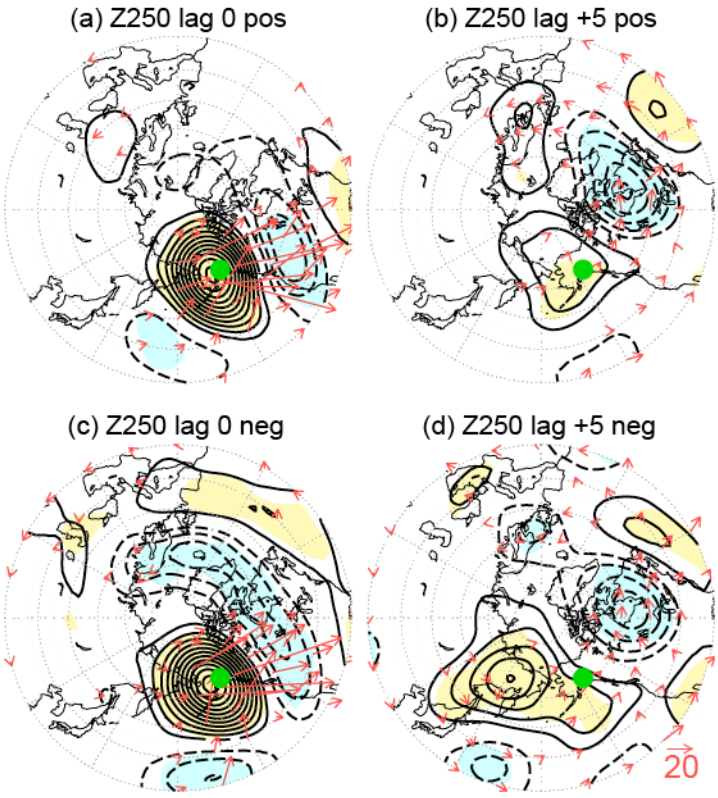

Figure 8. (a) Same as in Fig. 2h, but for 10 BH events over Alaska (62.5°N, 215°E) that accompany strongest positive $[V^*T^*]_a$. (b) Same as in (a), but for the lag of +5 day. (c) Same as in (a), but for another 10 BH events that accompanies strongest negative $[V^*T^*]_a$. (d) Same as in (c), but for the lag +5 day.

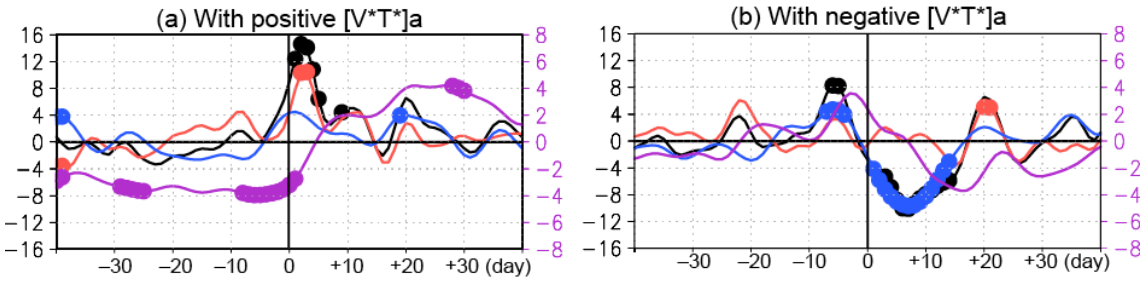

Figure 9. (a) As in Fig. 3a, but for 10 BH events over Alaska (62.5°N, 215°E) that accompany strongest positive $[V^*T^*]_a$. (b) As in (a), but for another 10 BH events that accompany strongest negative $[V^*T^*]_a$.

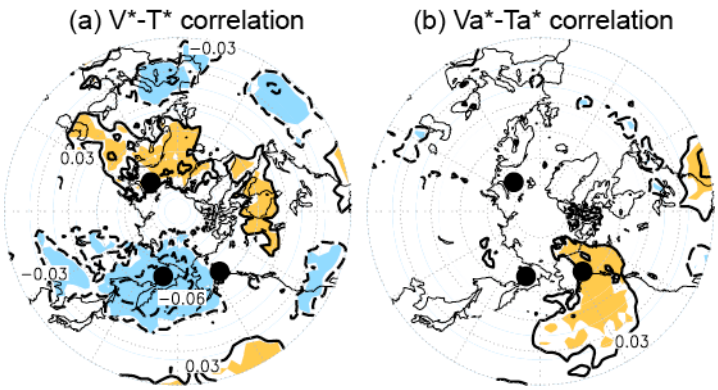

Figure 10. (a) As in Fig. 5a, but for composited anomalies for the pattern correlation between V^* and T^* over the domain poleward of 45°N at the 100-hPa level. (b) As in (a), but for pattern correlation between V_a^* and T_a^*.